JCE
JOURNAL OF CIVIL ENGINEERING
ISSN 2086 - 1206 E-ISSN 2579 - 9029

The Impact Of Tide On Flooding In The The Kali Welang, Pasuruan, East Java

Ainun M. M. Gasa[a*], Umboro Lasminto[a]

Correspondence

[a]Civil Engineering Department, Sepuluh Nopember Institute of Technology , ITS Campus, Surabaya 60111, Indonesia.

Corresponding author email adress: ainun992200@gmail.com

Submitted : 06 September 2025
Revised : 25 November 2025
Accepted : 28 November 2025

Abstract

Flooding in the Welang River, Pasuruan, East Java, is a recurrent problem influenced by multiple factors, primarily high-intensity rainfall and tidal fluctuations. This study aims to quantitatively assess the impact of tidal conditions—including extreme events such as supermoons—on the spatial extent and depth of flood inundation in the downstream segment of the Welang River. Utilizing hydrologic (HEC-HMS) and hydraulic (HEC-RAS) modeling, the research estimates design flood discharges for multiple return periods and simulates three scenarios: (1) flood discharge without tidal influence, (2) flood discharge under normal tidal conditions, and (3) flood discharge during tidal peaks associated with a supermoon. The results indicate that the 100-year design discharge reaches 409.7 m^3/s. Tidal conditions significantly amplify both the extent and depth of inundation, with the greatest increase in flood coverage observed at the 2-year return period (85.88%). Furthermore, the supermoon phenomenon intensifies flooding, producing the highest additional inundation extent during the 5-year return period (34.81%).

Keywords

Flood, Tidal, Supermoon, Welang River, HEC-HMS, HEC-RAS, Flood Inundation.

INTRODUCTION

The Welang River serves as a critical watercourse traversing both Pasuruan Regency and Pasuruan City in East Java Province. Its watershed covers an area of approximately 509.50 km^2, with a total channel length of 40.09 kilometers and contributions from around 21 tributaries [1,2,3]. The river basin exhibits a meandering pattern and an expanded morphology in its upstream region, both of which contribute to the complex hydrological behavior observed within the Welang watershed [1,2,3,4].

The downstream reaches of the Welang River particularly the districts of Kraton, Gadingrejo, and Ponjentrek have long been recognized as highly susceptible to flooding [5,6]. Defined as the overtopping of riverbanks that inundates low-lying areas, flooding constitutes one of the most disruptive natural hazards affecting communities in this region [7,8]. Historical records reveal recurrent flood events of varying inundation depths, including 50–70 cm in April 2019, 100–120 cm in January 2020, and as high as 15–150 cm in March 2022 [9,10,11].

The primary drivers of flooding along the Welang River are multifaceted in nature. Prolonged high-intensity rainfall serves as the principal trigger. In addition, sedimentation in the downstream reaches contributes to riverbed aggradation, which in turn reduces the flow capacity of the channel [12,13]. A significant compounding factor is the influence of tidal fluctuations. During high tide, a backwater effect emerges, impeding the downstream conveyance of river discharge. This obstruction not only leads to water accumulation and elevated flood stages within the river, but also hampers the performance of local drainage systems, ultimately amplifying both the spatial extent and duration of inundation in the affected areas [14]. In light of the considerable material and physical losses resulting from flooding, this study is directed toward the following objectives:

1. To determine the design flood discharge of the Welang River.
2. To evaluate the influence of tidal fluctuations on floodwater surface elevations.
3. To assess the impact of sea level rise on the spatial extent of flood inundation.

RESEARCH SIGNIFICANCE

The outcomes of this study are expected to offer insights into the most effective and applicable flood control strategies for the Welang River, with potential relevance for implementation in other flood-prone areas as well.

METHODOLOGY

This research was conducted through a series of systematic stages, encompassing literature review, data collection, analysis, and modeling, as illustrated in Figure 1.

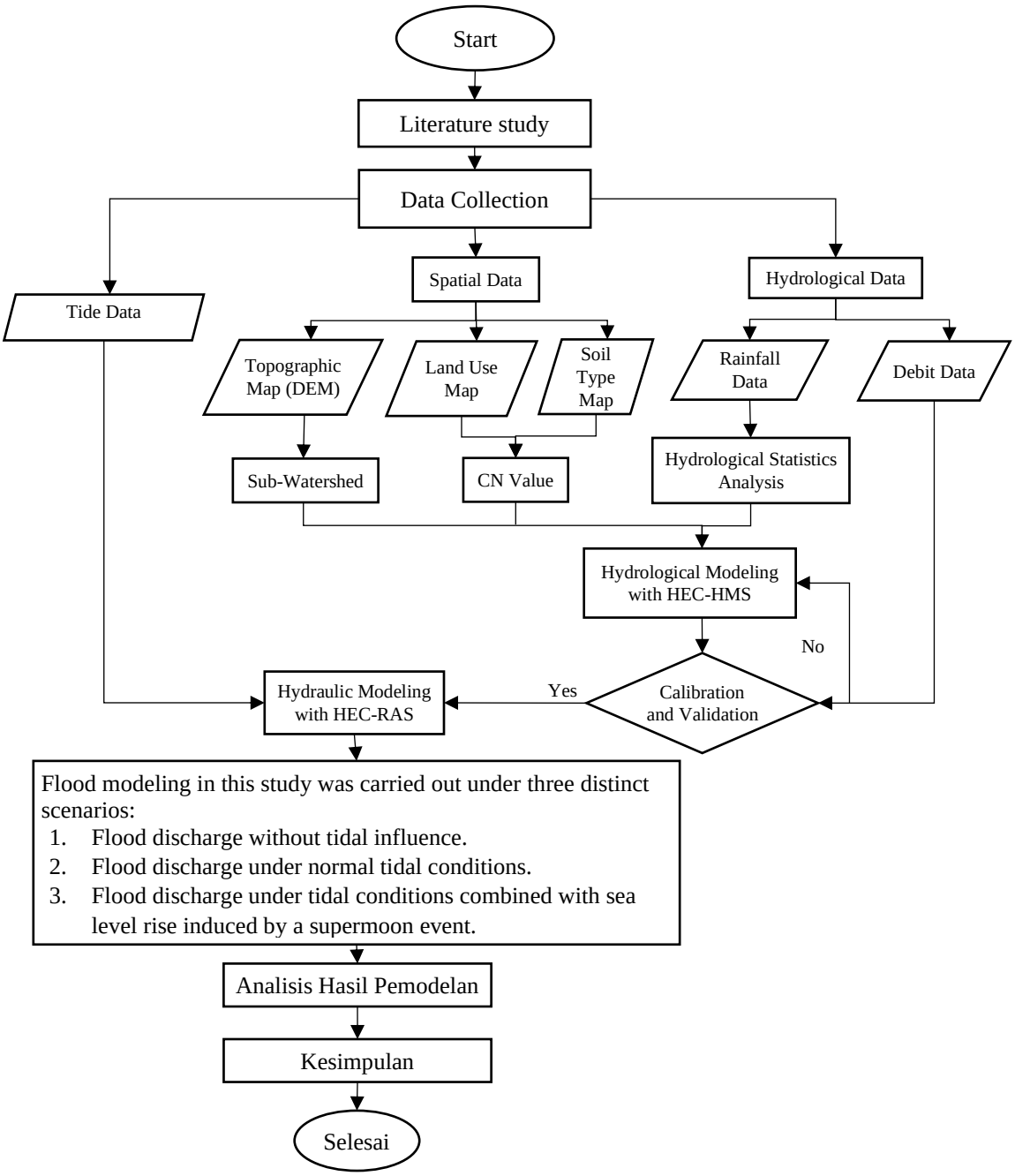

Figure 1 Research Flowchart

A. DATA COLLECTION AND ANALYSIS

The data utilized in this study comprised the following components:

1. Hydrological Data: Daily rainfall data (2003–2023) obtained from seven rain gauge stations, and daily discharge records (2002–2023).
2. Spatial Data: Topographic maps (Digital Elevation Model/DEM), land use maps, and soil type maps.
3. Tidal Data: Sea level fluctuation data sourced from the Geospatial Information Agency (Badan Informasi Geospasial/BIG) for the period 2019–2024.

The regional rainfall analysis was conducted using the Thiessen Polygon Method, followed by frequency analysis to estimate design rainfall for various return periods [15]. Among the distribution models tested, Normal, Log-Normal, Gumbel, and Log Pearson Type III, the Gumbel distribution was identified as the most appropriate, based on goodness-of-fit evaluations using the Chi-Square and Smirnov–Kolmogorov tests [16].

1. Normal Distribution

$$X_t = \bar{x} + K_t S$$

Explanation:
X_t = rain height plan for a repeat period (mm/day)
$\bar{x}$ = average maximum rainfall value (mm/day)
S = standard deviation
Kt = normal distribution frequency factor

2. Log Normal Distribution

$$X_t = 10^{\log x + K_t \cdot S}$$

3. Gumbel Distribution

$$X_t = x + \frac{(Y_t - Y_n)}{S_n} \cdot S$$

Explanation:

X_t = rain height plan for a repeat period (mm/day)
$\bar{x}$ = average maximum rainfall value (mm/day)
S = standard deviation
Y_t = reduced variable
Y_n = reduced mean
S_n = reduced standard deviation

4. Log Pearson Tipe III Distribution

$$X_t = 10^{\log x + K \cdot S}$$

Subsequently, hourly rainfall distribution was derived to address the absence of observed sub-daily precipitation data in the study area, including the Welang River Basin. Daily rainfall records were disaggregated into hourly values using the Mononobe method, accompanied by the assignment of appropriate distribution coefficients. The estimation of hourly rainfall intensity was carried out based on an assumed storm duration of six hours [17,18,19,20].

Rainfall Distribution Formula Mononobe Model

$$R_T = \left\{\frac{R_{24}}{t}\right\} \times \left\{\frac{t}{T}\right\}^{2/3}$$

Explanation:

R_T = Average Rainfall Intensity in T hours (mm/Hour)
R_{24} = Effective Rainfall in One Day (mm)
T = Start Time of Rain (hour)
t = Rain Concentration Time (hours), (for Indonesia t = 6 hours)

B. HYDROLOGICAL MODELING (HEC-HMS)

The HEC-HMS (Hydrologic Modeling System) software was employed to simulate rainfall–runoff processes. This model aims to transform design rainfall into flood hydrographs for various return periods (Q2, Q5, Q10, Q25, Q50, and Q100) [21,28]. Key model parameters, such as Curve Number (CN) and lag time, were determined based on the physical characteristics of the watershed, derived from spatial datasets. The modeling process involved calibration and validation to ensure that the model accurately represented field hydrological conditions [28]. Calibration was performed by comparing model outputs against observed discharge data from two major flood events: 28 April 2019 and 21 January 2022. Parameter adjustments continued until the simulation satisfied statistical performance criteria based on the Coefficient of Determination (R^2), Root Mean Square Error (RMSE), and Nash–Sutcliffe Efficiency (NSE) [22] (see Table 1).

Table 1. HEC-HMS Performance Ratings for Summary Statistics

Performance Rating	NSE	RSR	R^2
Very Good	$0.75 < NSE \leq 1.00$	$0.00 < RSR \leq 0.50$	$R^2 \geq 0.85$
Good	$0.65 < NSE \leq 0.75$	$0.50 < RSR \leq 0.60$	$0.70 \leq R^2 < 0.85$
Satisfactory	$0.50 < NSE \leq 0.65$	$0.60 < RSR \leq 0.70$	$0.50 \leq R^2 < 0.70$
Unsatisfactory	$NSE \leq 1.00$	$RSR > 0.70$	$R^2 \leq 0.85$

C. HYDRAULIC MODELING (HEC-RAS)

2D hydraulic modeling using HEC-RAS was employed to simulate the extent and depth of flood inundation under three distinct scenarios [23,24,25]:

1. Scenario I : Flood discharge without tidal influence.
2. Scenario II : Flood discharge under normal tidal conditions.
3. Scenario III : Flood discharge under tidal conditions intensified by sea level rise during a supermoon event.

RESULTS AND DISCUSSIONS

A. HYDROLOGICAL ANALYSIS AND PLANNED FLOOD DISCHARGE

1. The Spatial Rainfall Analysis

The spatial rainfall analysis within the Welang River Basin was conducted using the Thiessen Polygon Method, based on data from seven rainfall stations. The resulting area-weighting coefficients for each station are presented in Table 2.

Table 2. Calculation of Thiessen Polygon Area at the Welang Watershed

No	Rain Station Post Name	Wide (Km^2)	Contribution (%)
1	Tutur	87.887	17.88
2	Lawang	101.932	20.73
3	Purwosari	57.116	11.62
4	Selowongso	63.655	12.95
5	Pager	72.945	14.84
6	Telebok	33.739	6.86
7	Wonorejo	74.364	15.13
	Total	**491.638**	**100**

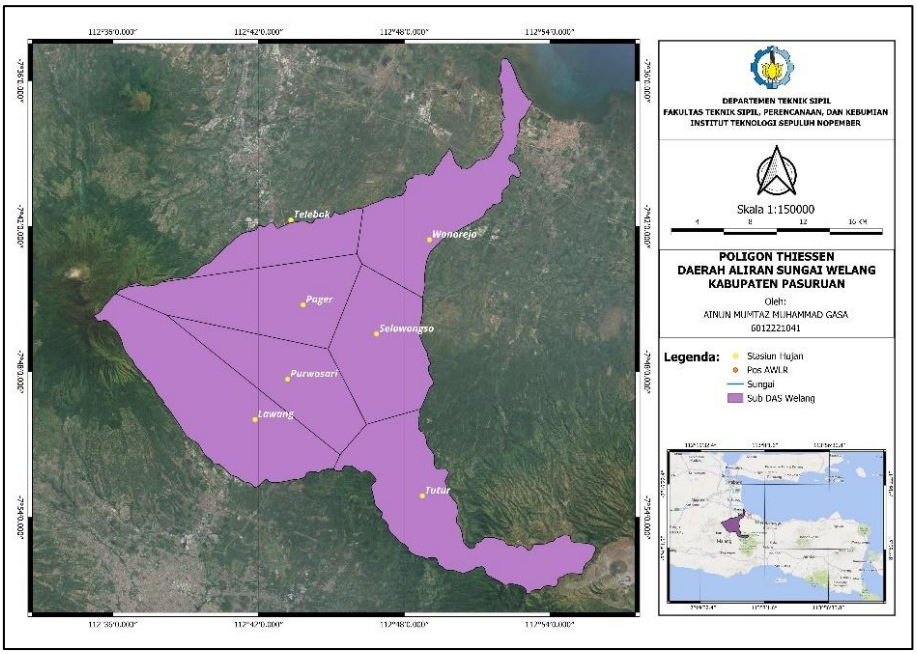

Figure 2. Thiessen Polygon in the Welang Watershed with 7 Rain Stations

Table 3. Annual Maximum Daily Rainfall

MODEL			
Year	**Rmax (mm)**	**Year**	**Ri (mm)**
2003	47.27	2008	77.87
2004	70.79	2010	76.98
2005	40.24	2016	76.19
2006	48.92	2004	70.79
2007	40.15	2021	70.72
2008	77.87	2019	66.30
2009	53.31	2015	59.68
2010	76.98	2011	59.40
2011	59.40	2009	53.31
2012	42.26	2017	53.09
2013	50.07	2014	52.20
2014	52.20	2020	50.95
2015	59.68	2013	50.07
2016	76.19	2006	48.92
2017	53.09	2003	47.27
2018	38.18	2023	46.21
2019	66.30	2022	42.37
2020	50.95	2012	42.26
2021	70.72	2005	40.24
2022	42.37	2007	40.15
2023	46.21	2018	38.18

Table 3 presents data on the maximum daily rainfall observed between 2003 and 2023. The highest recorded value during this 21-year period was 77.87 mm, which occurred in 2008, while the lowest maximum daily rainfall was 38.18 mm, recorded in 2018. The data exhibit notable interannual variability, with several years showing exceptionally high daily rainfall maxima (e.g., 2008, 2010, 2016) and others displaying relatively lower values (e.g., 2018, 2007, 2005).

2. Analysis of Rainfall Frequency

The threshold values and calculation results for each distribution method are presented in Table 4. Based on the evaluation outcomes, the Gumbel and Log Pearson Type III distributions were identified as meeting the required statistical criteria.

Table 4. Parameter Requirement Values for Each Distribution Method

No	Metode	Requirements		Result		Explanation
1	Gumbel	$Cs \leq 1.1369$	1.14	Cs	0.518	Fulfill
		$Ck \leq 5.4002$	5.4	Ck	2.365	Fulfill
2	Normal	$Cs \approx 0$	0	Cs	0.518	Not Fulfilled
		$Ck = 3.0$	3	Ck	2.365	Not Fulfilled
3	Log Pearson III	$Cs \neq 0$		Cs	0.249	Fulfill
4	Log Normal	$Cs = Cv^3 + 3Cv$	0.718	Cs	0.249	Not Fulfilled
		$Ck = Cv8 + 6Cv6 + 15Cv4 + 16Cv^2 + 3$	3.054	Ck	0.000	Not Fulfilled

Subsequently, the distribution methods that satisfied the selection criteria were subjected to goodness-of-fit testing using the Chi-Square and Smirnov–Kolmogorov tests.

Table 5. Calculation of Chi Square Goodness of Fit Test on the Log Pearson III Distribution Method

Class	P	Tr	KTr	Rtr	Limit Value of Each Class			Ei	Oi	((Ei - Oi)^2)/Ei
1	0,167	6	0,922	66,768		>	66,768	3,50	5	0.643
2	0,333	3	0,248	57,164	57,164	-	66,768	3,50	3	0.071
3	0,500	2	-0,041	53,480	53,480	-	57,164	3,50	0	3.500
4	0,667	1,5	-0,581	47,223	47,223	-	53,480	3,50	7	3.500
5	0,833	1,2	-1,120	41,709	41,709	-	47,223	3,50	3	0.071
6	1,000	1				<	41,709	3,50	3	0.071
						Total		21	21	7.857

Table 6. Calculation of Chi Square Goodness of Fit Test on Gumbel Distribution Method

Class	P	Tr	KTr	Rtr	Limit Value of Each Class			Ei	Oi	((Ei - Oi)^2)/Ei
1	0,167	6	1.650	69.077		>	69.077	3,50	5	0.643
2	0,333	3	0.744	58.054	58.054	-	69.077	3,50	3	0.071
3	0,500	2	0.367	53.456	53.456	-	58.054	3,50	0	3.500
4	0,667	1,5	-0.094	47.850	47.850	-	53.456	3,50	6	1.786
5	0,833	1,2	-0.583	41.897	41.897	-	47.850	3,50	4	0.071
6	1,000	1				<	41.897	3,50	3	0.071
						Total		21	21	6,143

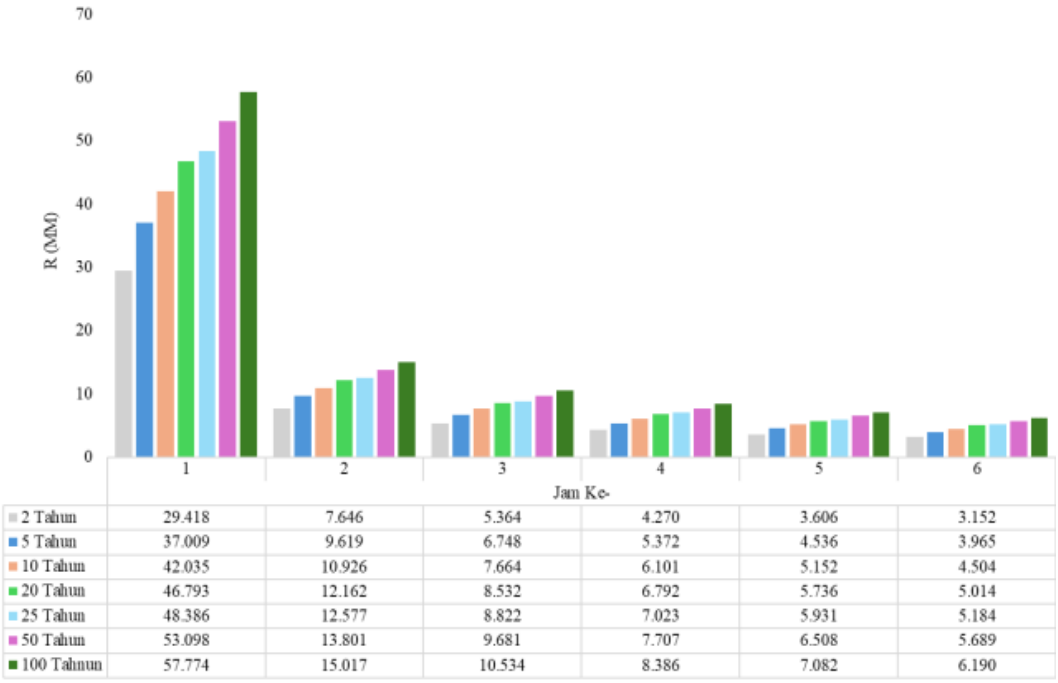

2 Tahun	29.418	7.646	5.364	4.270	3.606	3.152
5 Tahun	37.009	9.619	6.748	5.372	4.536	3.965
10 Tahun	42.035	10.926	7.664	6.101	5.152	4.504
20 Tahun	46.793	12.162	8.532	6.792	5.736	5.014
25 Tahun	48.386	12.577	8.822	7.023	5.931	5.184
50 Tahun	53.098	13.801	9.681	7.707	6.508	5.689
100 Tahnun	57.774	15.017	10.534	8.386	7.082	6.190

Figure 3. Hourly Rain Values for Each Recurrence Period

Based on the frequency analysis, the Gumbel distribution was selected as the most suitable model. The Chi-Square goodness-of-fit test yielded a calculated Chi-Square value of 6.143, which is less than the critical value of 7.815, thereby confirming the acceptance of this distribution method.

3. Hourly Rainfall Distribution

Rainfall intensity was analyzed across multiple return periods. Based on the results, peak rainfall occurred during the first hour and gradually decreased until the sixth hour. The hourly distribution of rainfall depths for each return period is illustrated in Figure 3.

B. HYDROLOGICAL MODELING HEC-HMS

Rainfall–runoff modeling using HEC-HMS was conducted based on daily precipitation inputs and parameters calibrated to reflect field conditions. The simulation employed the following computational methods and model components:

Precipitation : Specified Hyetograph
Loss Method : SCS curve number
Baseflow Methods : Constant monthly
Transform Method : SCS UH
Routing Methods : Lag

The initial parameter values for the HEC-HMS hydrological model of the Welang River Basin were derived from analyses of Digital Elevation Models, land use patterns, and soil types. Input parameters encompassed hydrological loss, transform, baseflow, and routing components. The model was first applied to the Welang Basin, where a stream gauge station is located at the designated outlet point to serve as a reference for calibration. A schematic of the HEC-HMS modeling configuration is presented in Figure 4 [21,22,28].

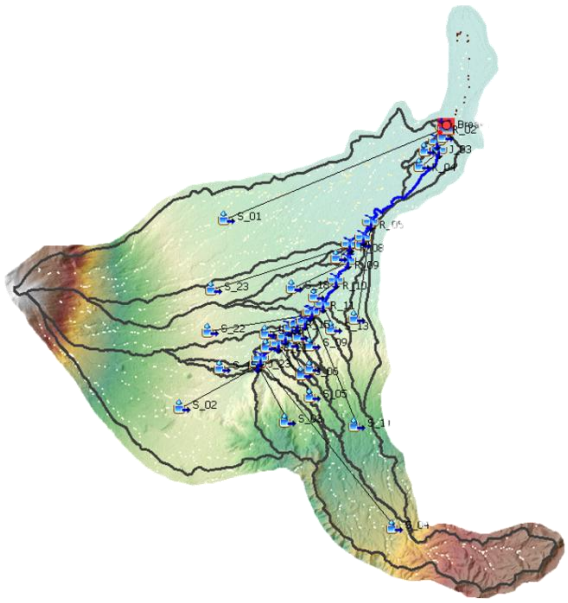

Figure 4. Modeling HEC HMS

1. Loss Method

The parameters applied in the loss method using the SCS Curve Number (CN) approach include the CN value, percentage of impervious area, and initial abstraction (Ia). The values of these three loss parameters used in the hydrological model of the Welang River Basin are presented in Table 7.

Table 7. Initial Parameter Values for the SCS CN Loss Method

Sub-Basin	CN	S	IA (*Initial Abstraction*)	% *Impervious*
1	81	59.58	11.92	10.65
2	81	59.58	11.92	10.84
3	79	67.52	13.5	8.42
4	80	63.5	12.7	10.33
5	79	67.52	13.5	8.34
6	79	67.52	13.5	8
7	81	59.58	11.92	10.43
8	80	63.5	12.7	8.27
9	79	67.52	13.5	10.47
10	79	67.52	13.5	9.18
11	80	63.5	12.7	9.11
12	80	63.5	12.7	10.18
13	81	59.58	11.92	9.45
14	81	59.58	11.92	11.38
15	81	59.58	11.92	11.05
16	78	71.64	14.33	9.14
17	80	63.5	12.7	10.77
18	80	63.5	12.7	10.4
19	80	63.5	12.7	9.07
20	80	63.5	12.7	12.07
21	80	63.5	12.7	10.19
22	79	67.52	13.5	10.02
23	80	63.5	12.7	9.94
24	80	63.5	12.7	9.55
25	77	75.87	15.17	8.09

2. Baseflow Method

The baseflow component was modeled using the Constant Monthly method, wherein the lowest recorded monthly discharge 0.001849 m^3/s was applied. This value corresponds to observations from July in both 2021 and 2022. The baseflow configuration is illustrated in Figure 5.

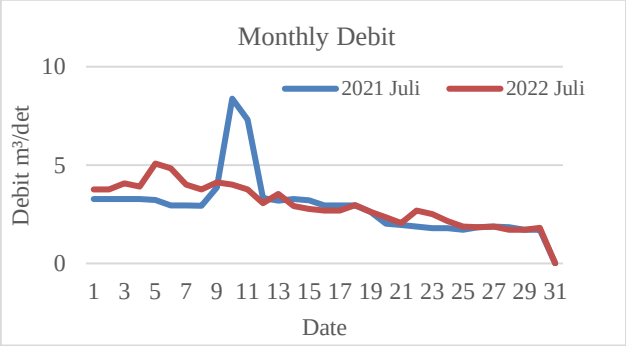

Figure 5. Debit for July 2021 and 2022

3. Transform Method

The SCS Unit Hydrograph method incorporates two primary parameters: lag time and Peak Rate Factor (PRF). In the implementation of this method, watershed or basin slope influences only the lag time parameter. Meanwhile, a PRF value of 400 was adopted, corresponding to the model's classified slope category of 10–20%, with an observed slope of 12.67% [26]. These parameter values are presented in Table 9.

Table 9. Table for Determining PRF Value

Slope (%)	PRF
0-15 %	100
1.5-4.5 %	200
4.5-10 %	300
10-20 %	400
>20 %	575

Lag time values for each sub-watershed were computed using the Lag method, as outlined in the HEC-HMS Technical Reference Manual. The calculated lag time for each sub-basin is presented in Table 10.

4. Routing Method

The routing method employed in this study is the Lag method, which is widely applied in hydrological modeling and hydrograph simulations using HEC-HMS. The initial simulation involved calculating lag time values using the Kirpich equation (1940). The computed lag time values for each river reach are presented in Table 11.

Table 10. Lag Time Values for Each Sub-Watershed

Sub-Basin	L (Km)	CN	S (inch)	Y (mm)	Y(%)	L(ft)	Tc	Lag (hour)	Lag (Minute)
1	40.66	81	2.35	0.12	11.55	133414.3	7.57	4.54	272.6
2	19.64	81	2.35	0.14	13.59	64445.2	3.90	2.34	140.4
3	11.27	79	2.66	0.26	26.21	36968.6	1.92	1.15	69.0
4	33.72	80	2.50	0.29	28.53	110644.6	4.28	2.57	154.1
5	9.63	79	2.66	0.20	19.60	31582.6	1.95	1.17	70.3
6	4.78	79	2.66	0.15	14.82	15686.7	1.28	0.77	46.2
7	1.92	81	2.35	0.15	15.07	6294.3	0.58	0.35	20.7
8	6.66	80	2.50	0.17	17.18	21860.6	1.51	0.90	54.3
9	1.96	79	2.66	0.14	13.87	6435.2	0.65	0.39	23.4
10	3.32	79	2.66	0.15	15.38	10904.7	0.94	0.57	33.9
11	19.73	80	2.50	0.17	16.50	64736.0	3.67	2.20	132.0
12	14.83	80	2.50	0.11	10.93	48657.9	3.58	2.15	129.0
13	5.11	81	2.35	0.12	12.42	16774.4	1.39	0.83	50.0
14	8.28	81	2.35	0.07	7.36	27160.0	2.65	1.59	95.5
15	5.95	81	2.35	0.08	7.73	19537.0	1.99	1.19	71.6
16	2.79	78	2.82	0.12	12.41	9163.3	0.94	0.56	33.9
17	5.30	80	2.50	0.07	7.02	17384.8	1.96	1.18	70.7
18	10.84	80	2.50	0.07	6.53	35552.7	3.61	2.17	129.9
19	2.62	80	2.50	0.05	5.49	8583.6	1.26	0.76	45.4
20	2.93	80	2.50	0.05	4.96	9605.4	1.45	0.87	52.3
21	7.53	80	2.50	0.09	8.62	24698.3	2.35	1.41	84.5
22	19.49	79	2.66	0.21	20.78	63939.1	3.34	2.00	120.1
23	15.85	80	2.50	0.11	10.68	52015.7	3.82	2.29	137.7
24	4.59	80	2.50	0.05	4.75	15072.4	2.13	1.28	76.7
25	3.60	77	2.99	0.05	4.89	11812.9	1.89	1.14	68.1

Table 11. Lag Time Values on Rivers with the Kirpich Equation (1940)

Reach	L(km)	L (m)	L (ft)	S	S (%)	Tc	tp (minutes)
R_23	0.091	91.47	300.10	0.00953	0.95	3.79	2.27
R_22	0.523	522.81	1715.26	0.01565	1.57	11.97	7.18
R_21	1.695	1695.03	5561.12	0.04909	4.91	19.08	11.45
R_20	0.048	48.47	159.02	0.0229	2.29	1.66	0.99
R_19	0.675	674.85	2214.07	0.01721	1.72	14.05	8.43
R_18	0.075	75.43	247.47	0.00493	0.49	4.21	2.52
R_17	0.373	373.12	1224.15	0.01937	1.94	8.51	5.10
R_16	0.794	793.53	2603.44	0.01883	1.88	15.38	9.23
R_15	0.537	536.58	1760.43	0.00828	0.83	15.61	9.37
R_14	0.683	682.58	2239.44	0.01075	1.08	16.99	10.20
R_13	1.020	1020.32	3347.51	0.01281	1.28	21.64	12.99
R_12	0.162	162.03	531.59	0.01565	1.57	4.86	2.92
R_11	1.102	1101.66	3614.37	0.01017	1.02	25.10	15.06
R_10	2.170	2169.85	7118.93	0.01184	1.18	39.89	23.93
R_09	1.877	1877.28	6159.06	0.00854	0.85	40.46	24.28
R_08	1.466	1465.78	4808.99	0.00792	0.79	34.43	20.66
R_07	0.067	67.12	220.21	0.00606	0.61	3.55	2.13
R_06	1.440	1439.65	4723.26	0.0059	0.59	38.03	22.82
R_05	1.299	1298.87	4261.38	0.00705	0.71	32.80	19.68
R_04	8.763	8763.12	28750.39	0.00442	0.44	170.76	102.46
R_03	0.629	628.89	2063.29	0.00455	0.46	22.21	13.33
R_02	1.297	1297.44	4256.69	0.0036	0.36	42.46	25.47
R_01	0.260	259.56	851.57	0.00074	0.07	22.61	13.57

Subsequent HEC-HMS modeling was performed for two major flood events 28 April 2019 and 21 January 2022 as part of the calibration process wherein simulated discharge outputs were compared against observed flow data to ensure the model's accuracy.

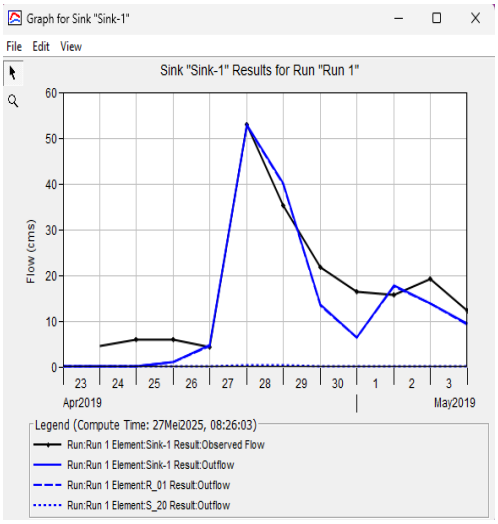

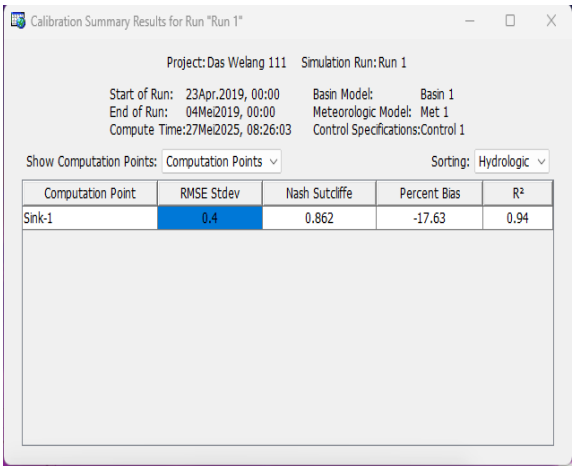

Figure 6. Calibration Flow Rate Chart from April 23 to May 4, 2019

The calibration results indicate a coefficient of determination (R^2) of 0.94, a root mean square error (RMSE) standard deviation of 0.4, and a Nash–Sutcliffe Efficiency (NSE) of 0.862 all of which fall within the 'Very Good' performance classification.

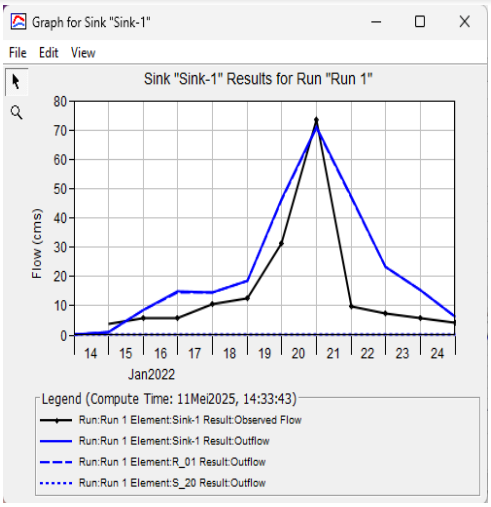

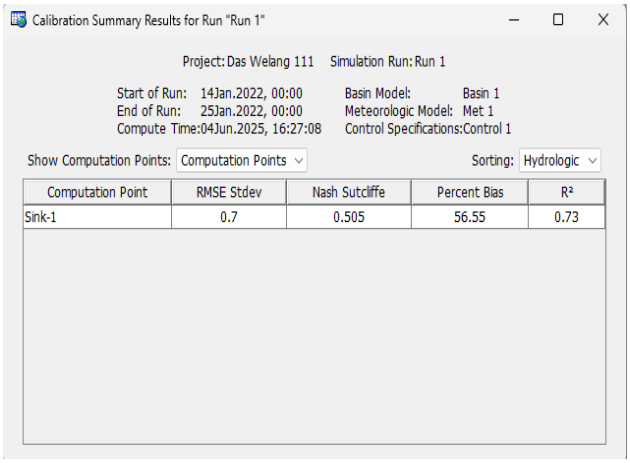

Computation Point	RMSE Stdev	Nash Sutcliffe	Percent Bias	R^2
Sink-1	0.7	0.505	56.55	0.73

Figure 7. Calibration Flow Rate Chart January 14 – 25, 2022

The calibration results yielded a coefficient of determination (R^2) of 0.73, a root mean square error (RMSE) standard deviation of 0.7, and a Nash–Sutcliffe Efficiency (NSE) of 0.505—all of which indicate acceptable to satisfactory model performance.

Following the calibration of the HEC-HMS model, design flood discharge simulations w
ere carried out. The resulting peak discharges for each return period are presented in Table 12, while the corresponding hydrographs are illustrated in Figure 8.

Table 12. Planned Peak Flood Discharge Values at the Downstream of Welang River

Recurrent period (Years)	Peak Debit (m^3/det)	Rush Hour
2	135.6	08:00
5	191.5	08:00
10	235.2	08:00
20	282.6	08:00
25	299.9	09:00
50	353.7	09:00
100	409.7	09:00

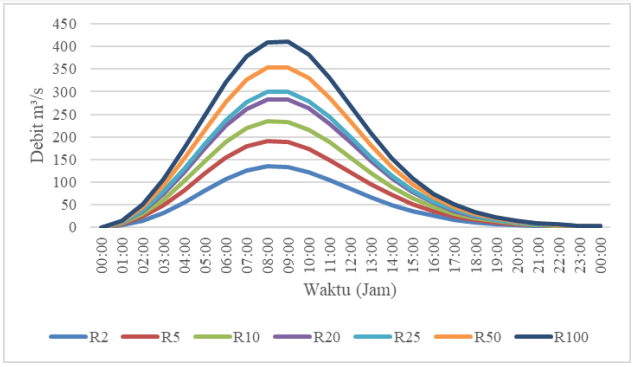

Figure 8. Results of Rainfall Modeling for Period of Return of the Welang Watershed

C. TIDAL DATA ANALYSIS

Tidal data obtained from the Geospatial Information Agency (BIG) indicate a significant variation in sea surface elevation between normal tidal conditions and those occurring during a supermoon event [27]. On 1 April 2024 (normal condition), the maximum tidal height was recorded at 2.18 meters, whereas on 17 October 2024 (supermoon condition), the maximum tidal height reached 3.05 meters. This discrepancy served as the basis for defining downstream boundary conditions in Scenario II and Scenario III.

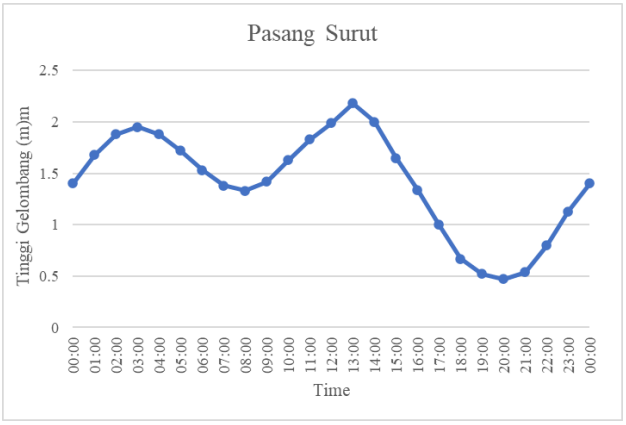

Figure 9. Tidal Data on April 1, 2024 (Normal)

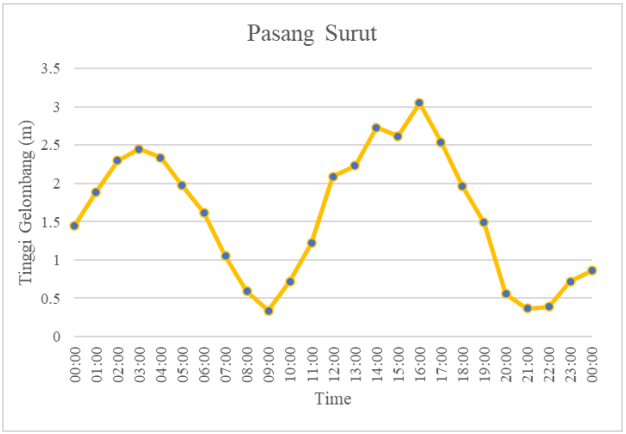

Figure 10. Tide Data on October 17, 2024 (Supermoon)

D. RESULTS OF FLOOD INUNDATION MODELING HEC-RAS

The results of the HEC-RAS simulation show a drastic difference between scenarios:

1. Scenario I (Without Tides)

In this scenario, flood inundation remained relatively confined to the riverbed and adjacent floodplains. Simulation results indicate that despite the substantial discharge, the absence of downstream tidal influence allowed water to flow relatively unimpeded.

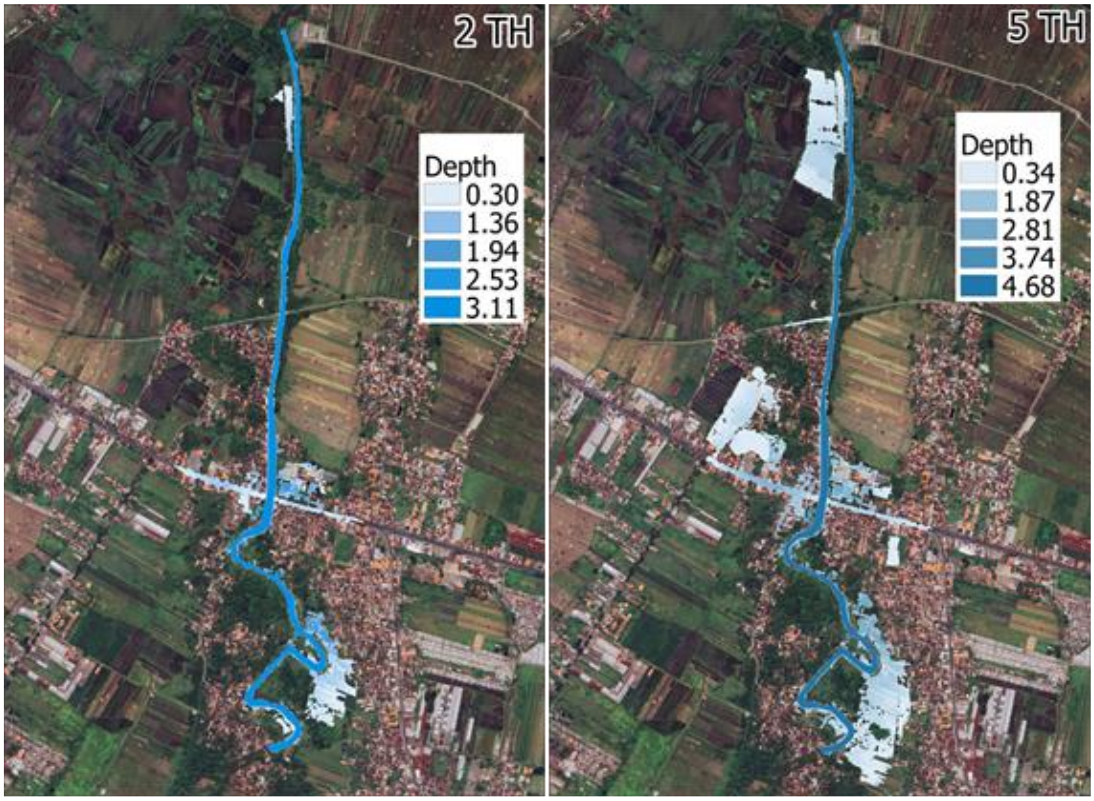

Figure 11. Area and depth of flood inundation scenario I part I

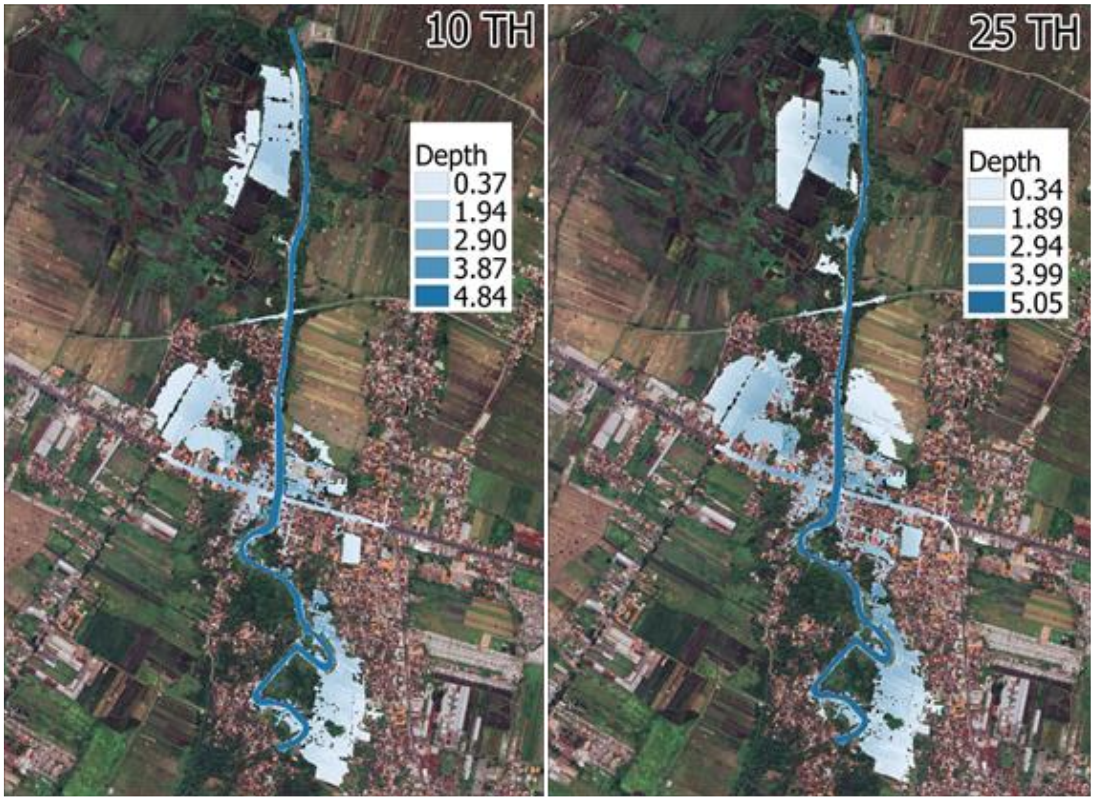

Figure 12. Area and depth of flood inundation scenario I part II

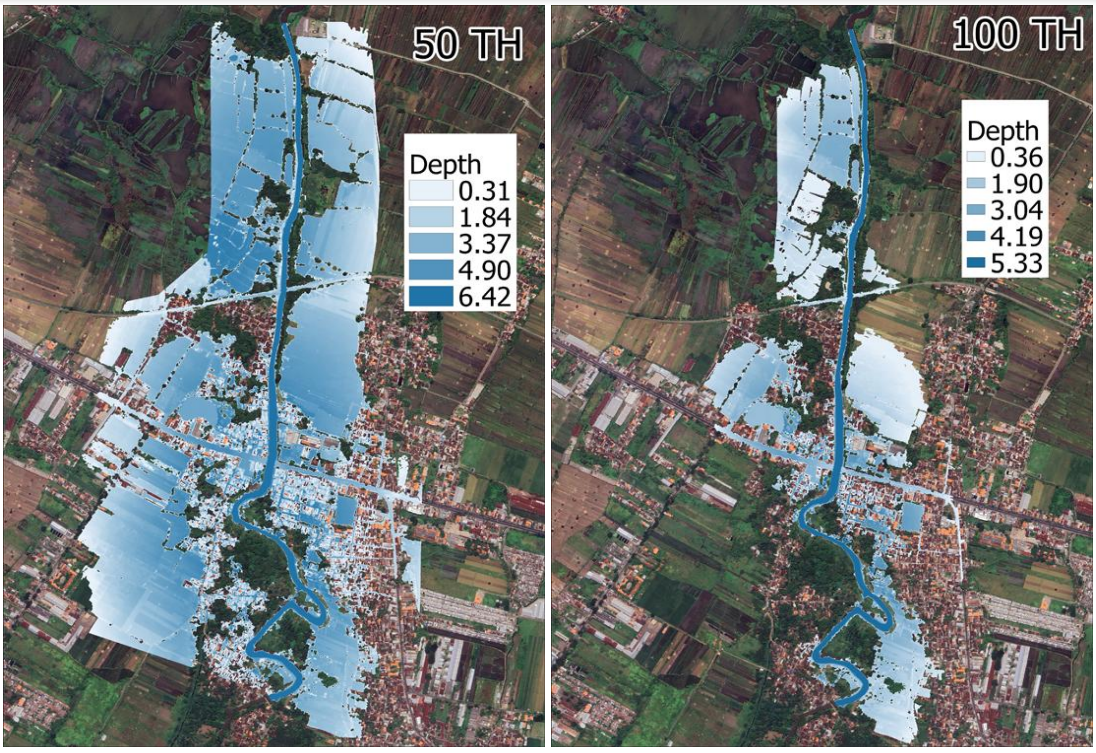

Figure 13. Area and depth of flood inundation scenario I part III

Table 13. Area and Depth of Flood Inundation Scenario I

Recurrent period	Area (km²)	Depth (m)
Q2	0.08	0.30 - 3.11
Q5	0.23	0.34 - 4.68
Q10	0.3	0.37 - 4.84
Q25	0.41	0.34 - 5.05
Q50	0.49	0.34 - 5.19
Q100	0.57	0.36 - 5.33

2. Scenario II (With Normal Tides)

The influence of normal tidal conditions markedly altered the flood inundation pattern. Downstream flow resistance caused water to back up and overflow further into the surrounding lowlands. The inundated area increased significantly across all return periods. For the 100-year flood (Q100), the inundation extent reached 1.53 km², with depths of up to 6.69 meters.

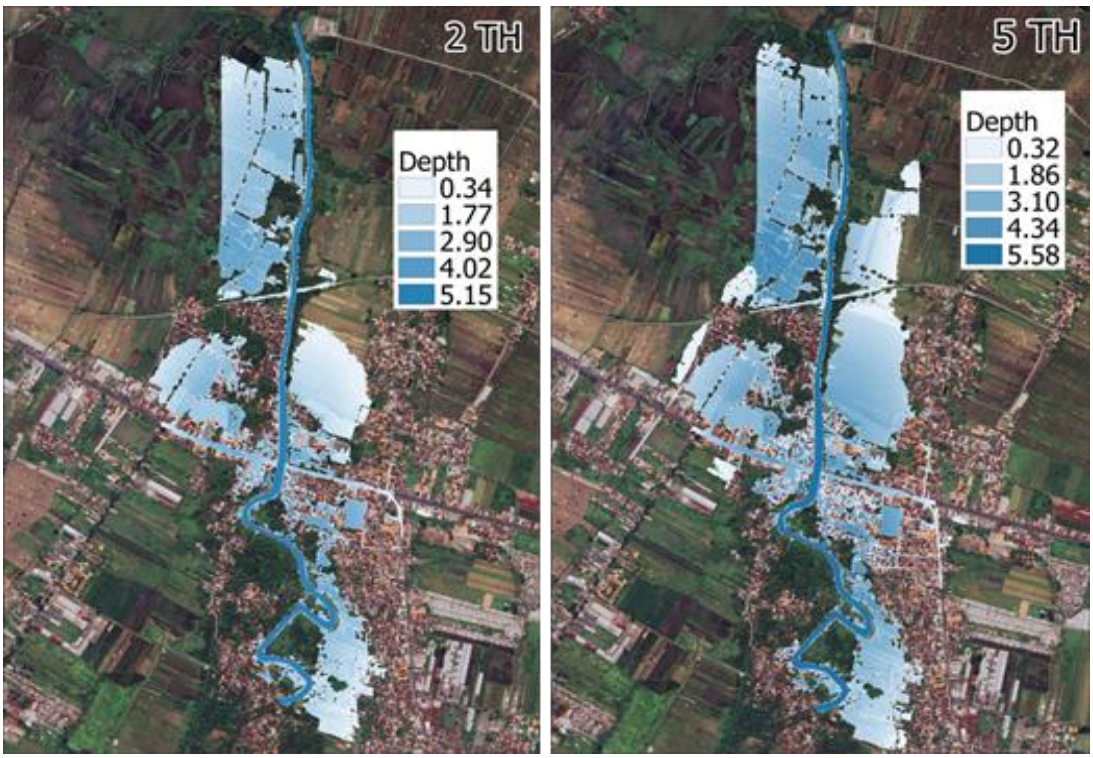

Figure 14. Area and depth of flood inundation scenario II part I

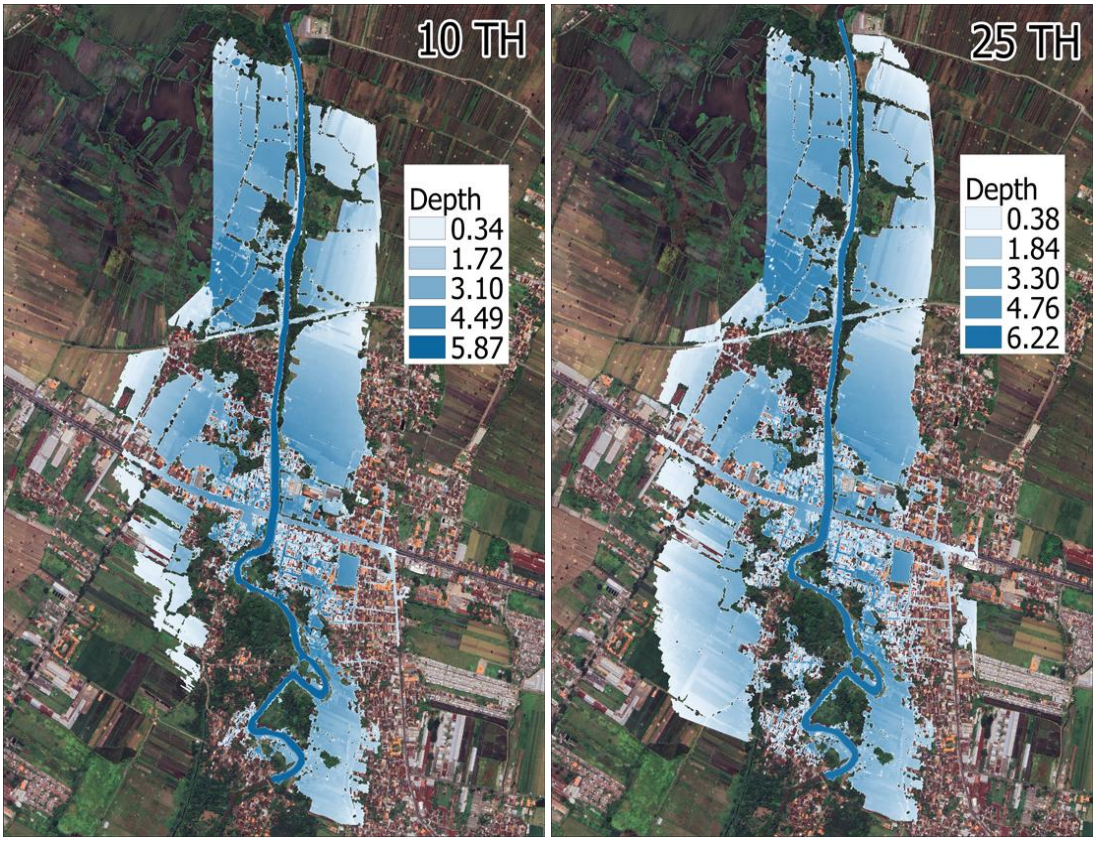

Figure 15. Area and depth of flood inundation scenario II part II

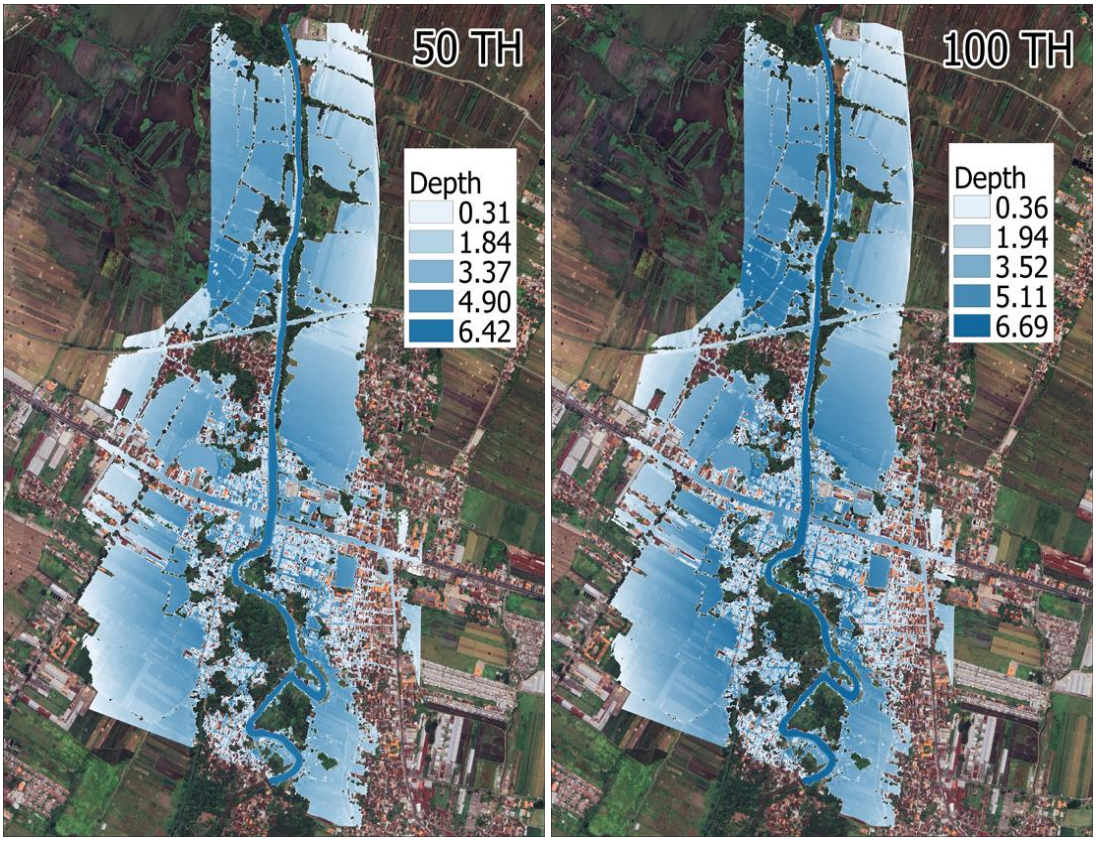

Figure 16. Area and depth of flood inundation scenario II part III

Table 14. Area and Depth of Flood Inundation Scenario II

Recurrent period	Area (km²)	Depth (m)
Q2	0.57	0.34 - 5.15
Q5	0.78	0.32 - 5.58
Q10	1	0.34 - 5.87
Q25	1.33	0.38 - 6.22
Q50	1.46	0.31 - 6.42
Q100	1.53	0.36 - 6.69

3. Scenario III (With Supermoon Tides)

This represents the worst-case scenario, wherein the peak tidal level induced by a supermoon coincides with flood discharge. The resulting inundation is the most extensive and deepest among all scenarios, indicating the highest level of risk for downstream areas. For the 100-year return period (Q100), the inundation extent reaches 1.73 km², with a maximum depth of 7.42 meters.

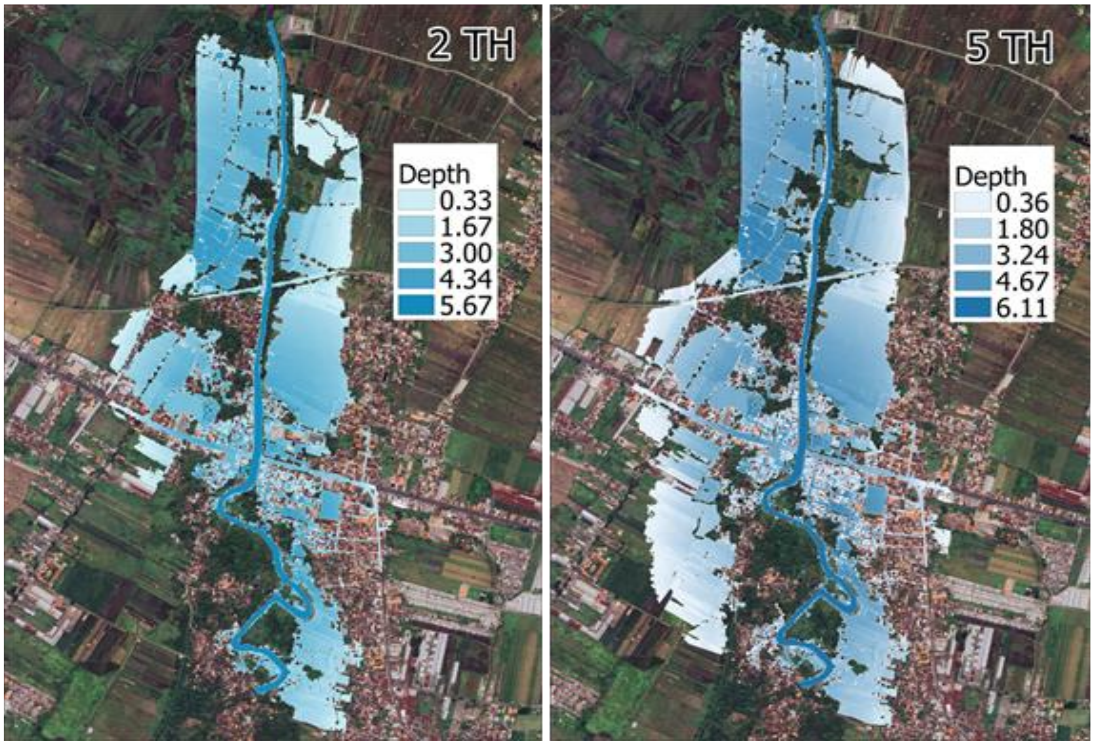

Figure 17. Area and depth of flood inundation scenario III part I

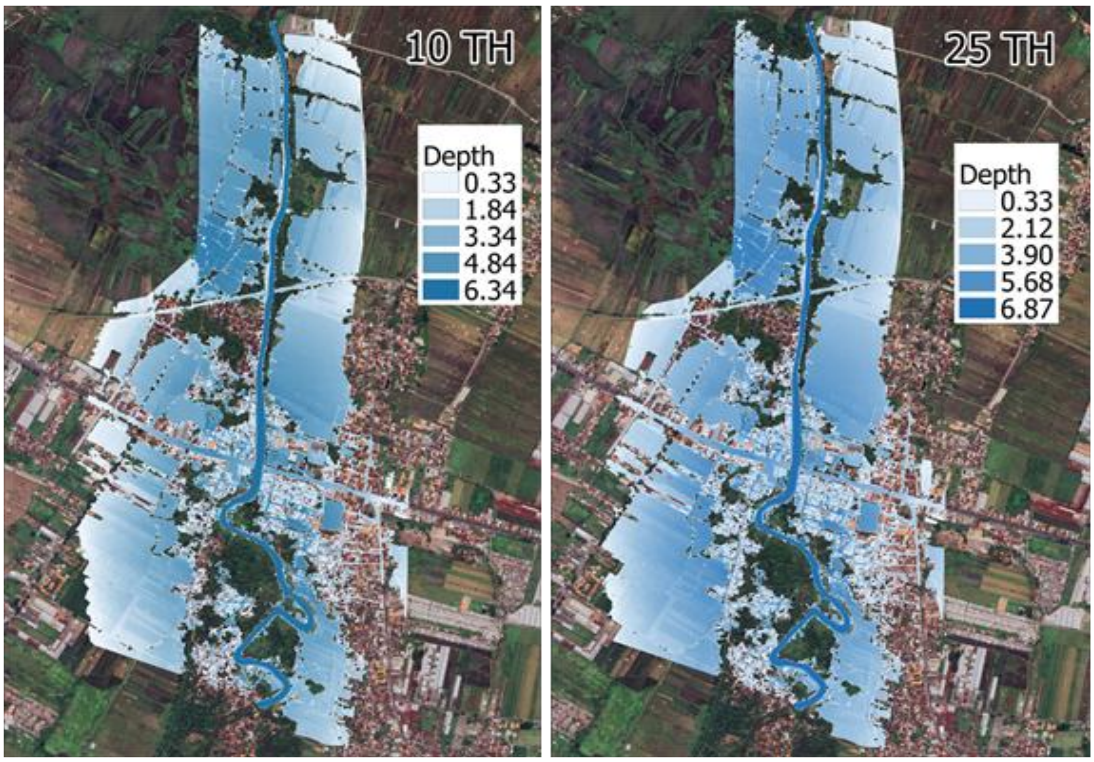

Figure 18. Area and depth of flood inundation scenario III part II

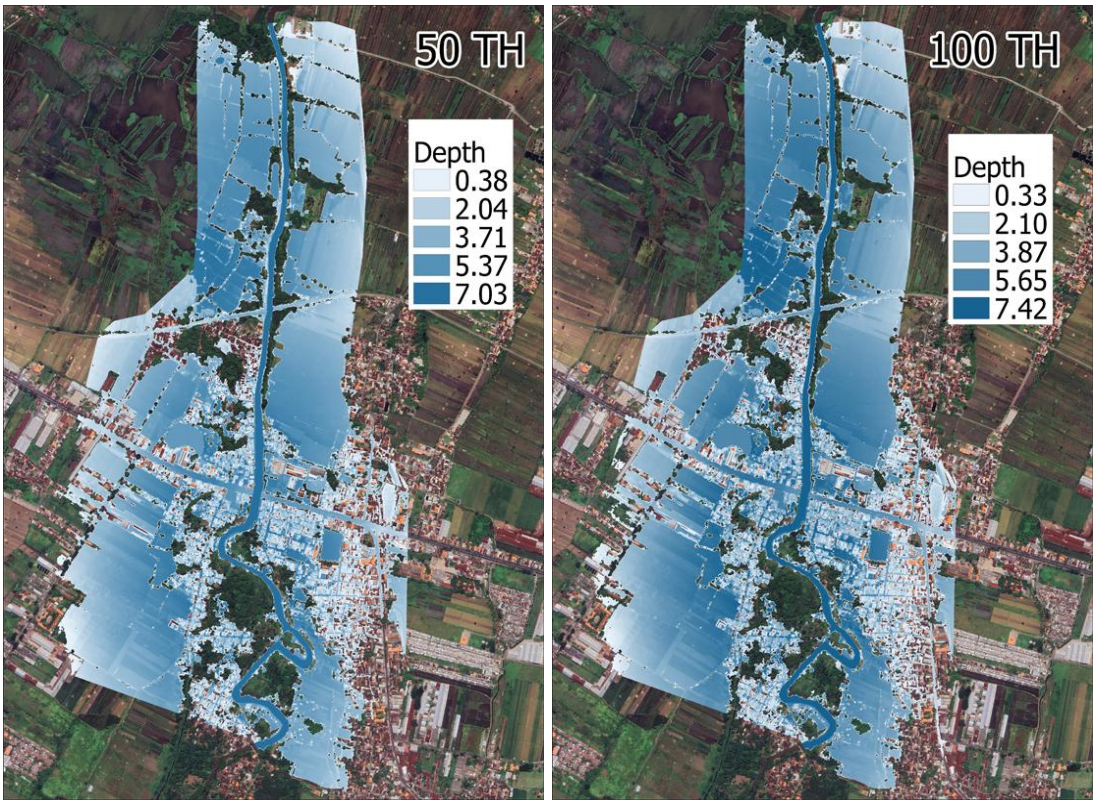

Figure 19. Area and depth of flood inundation scenario III part III

Table 15. Area and Depth of Flood Inundation Scenario III

Recurrent period	Area (km²)	Depth (m)
Q2	0.86	0.33 - 5.67
Q5	1.2	0.36 - 6.11
Q10	1.4	0.33 - 6.34
Q25	1.52	0.33 - 6.87
Q50	1.62	0.38 - 7.03
Q100	1.73	0.33 - 7.42

E. COMPARATIVE ANALYSIS

The comparative results of the three scenarios clearly demonstrate the escalating flood risk associated with tidal influences. Figures 11 and 12 summarize the differences in inundation extent and average water depth across the scenarios.

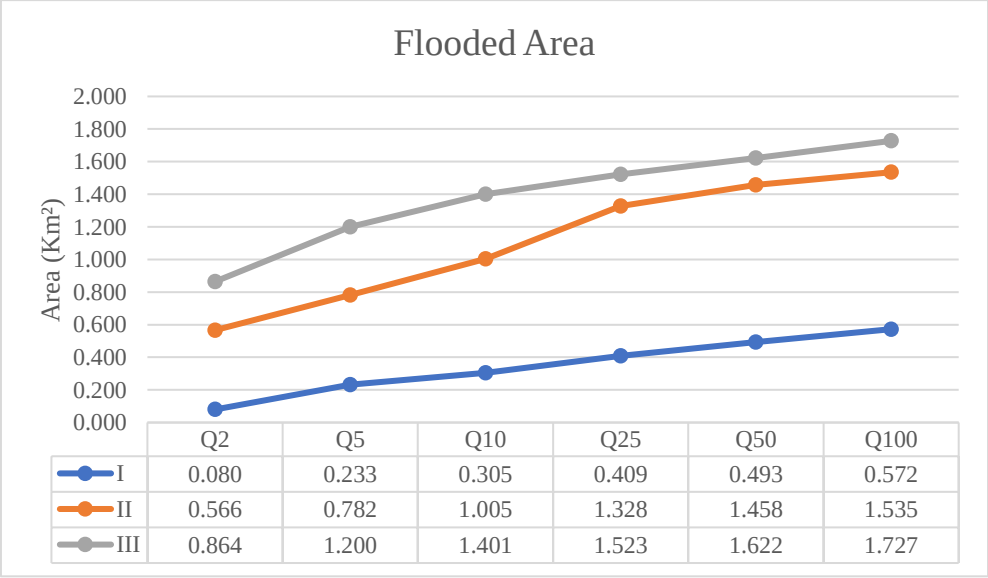

Figure 20 Comparison of Flooded Area for Three Scenarios

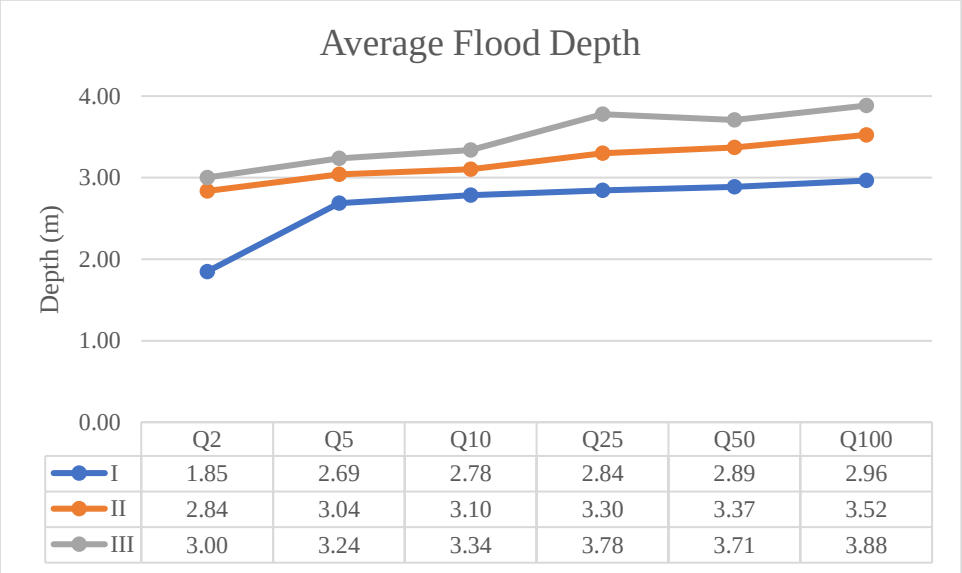

	Q2	Q5	Q10	Q25	Q50	Q100
I	1.85	2.69	2.78	2.84	2.89	2.96
II	2.84	3.04	3.10	3.30	3.37	3.52
III	3.00	3.24	3.34	3.78	3.71	3.88

Figure 21 Comparison of Average Flood Depth for Three Scenarios

The data allow for the following analysis:

- Impact of Normal Tides (Scenario I vs II): The extent of inundation increased dramatically, with the largest expansion observed for the Q2 return period an increase of 85.88% (from 0.08 km² to 0.57 km²). The greatest increase in flood depth also occurred under Q2 conditions, reaching 34.83%. These findings indicate that even under low discharge conditions, tidal influence plays a highly dominant role.
- Impact of Supermoon (Scenario II vs III): The rise in sea level due to the supermoon further increased both the extent and depth of inundation. The largest increase in flood extent was recorded for the Q5 return period, at 34.81% (from 0.78 km² to 1.20 km²), while the most significant rise in flood depth occurred under Q25 conditions, reaching 12.69%.

This analysis confirms that tidal fluctuations are a key controlling factor exacerbating downstream flooding along the Welang River. Astronomical phenomena such as the supermoon, which induces extreme tides, directly elevate the flood risk level in the affected region

CONCLUSIONS

This study aims to analyze the influence of tidal conditions and the supermoon phenomenon on flooding in the downstream area of the Welang River using hydrological and hydraulic modeling approaches. The methodology includes statistical rainfall analysis, hourly rainfall transformation, flood discharge modeling with HEC-HMS, and 2D hydraulic simulations using HEC-RAS under three tidal scenarios.

Based on the results of the analysis and modeling, the following conclusions can be drawn:

1. The design flood discharges at the downstream reach of the Welang River range from 135.6 m³/s (Q2) to 409.7 m³/s (Q100), with potential for widespread inundation due to the gentle riverbed slope.
2. Tidal fluctuations exert a significant influence by impeding downstream flow, thereby elevating water surface levels and expanding flood extent. In certain return periods, inundation areas increased by more than 85%.
3. Sea level rise associated with supermoon phenomena has been shown to substantially exacerbate flood inundation. The increase in flood extent under supermoon conditions may reach nearly 35% compared to normal tidal conditions.
4. This study affirms that any flood mitigation strategy for the Welang River must incorporate coastal hydrodynamics, particularly tidal processes and the potential for future sea level rise.

REFERENCES

[1] Khusnah, N., Kurniawan, D., & Prasetyo, T. E. (2021). Kajian karakter fisik dan hidrologi di Kali Welang Kecamatan Kraton Pasuruan. *Jurnal Rekayasa Sipil*, 10(2), 115–122.

[2] Rony, I. (2021), " *Inventarisasi Sumber air dan Anak Sungai Di Das Welang* ", *Sinkesjar*, Hal. 606–616

[3] Widjarnako, H. (2013). *Perencanaan Pengendalian Banjir Sungai Welang, Desa Sungiwetan Sampai Muara, Kabupaten Pasuruan* [Tugas Akhir, Institut Teknologi Sepuluh Nopember

[4] Supangat, A. B. (2012). Karakter hidrologi berdasarkan parameter morfometri DAS di kawasan Taman Nasional Meru Betiri. *Jurnal Penelitian Hutan dan Konservasi Alam*, 9(3), 275–283.

[5] Bilqis, Z. S. (2018). *Zonasi Risiko Bencana Banjir di Daerah Aliran Sungai Welang Kecamatan Kraton* [Tugas Akhir, Institut Teknologi Sepuluh Nopember]. Institut Teknologi Sepuluh Nopember Repository.

[6] Fitriani, D., Hidayati, S. N., & Purwanto, D. (2024). Studi pemetaan daerah rawan banjir berbasis Sistem

Informasi Geografis sebagai upaya mitigasi bencana pada DAS Welang. *Jurnal Teknologi dan Rekayasa Sumber Daya Air*, 4(2), 77–86.

[7] Pontoh, M. R. N., Walandouw, T. A., & Polii, B. (2021). Analisis kerentanan bencana banjir di Kabupaten Bolaang Mongondow Utara. *Jurnal Spasial*, 8(3), 153–160.

[8] Triatmodjo, B. (2013). *Hidrologi Terapan*. Yogyakarta: Beta Offset.

[9] Febriyanto, A., Hidayah, E., & Halik, G. (2018). Estimasi debit puncak DAS Welang di Kabupaten Pasuruan. *Jurnal Rekayasa Sipil dan Lingkungan*, 2(2), 141–150.

[10] PUSDA Jatim. (2020). *Final Draft Terms of Reference: Welang River Basin Flood Management and Master Plan*. Dinas Pekerjaan Umum Sumber Daya Air Provinsi Jawa Timur.

[11] BPBD Kabupaten Pasuruan. (2022). *Laporan Tahunan Penanggulangan Bencana Kabupaten Pasuruan 2019–2022*. Pasuruan: Pemerintah Kabupaten Pasuruan.

[12] Immanuella, L. A., Dermawan, V., & Winarta, B. (2022). Studi alternatif pengendalian banjir Sungai Welang dengan pendekatan pemodelan banjir aliran 2D. *Jurnal Teknik Pengairan*, 13(2), 245–257.

[13] Kurniawan, D. T., Prasetyorini, L., & Dermawan, V. (2024). Upaya mitigasi bencana banjir pada Sungai Welang di Kabupaten Pasuruan. *Jurnal Teknologi dan Rekayasa Sumber Daya Air*, 4(2), 88–97.

[14] Saputro, A. A., Hidayah, Z., & Wirayuhanto, H. (2023). Pemodelan dinamika arus permukaan laut alur pelayaran barat Surabaya. *Jurnal Kelautan*, 16(1), 1–10.

[15] Achmad, N., Widyasari, T., & Syaifullah, M. (2021). Analisis hujan wilayah dengan Metode Poligon Thiessen dan Isohyet di Kabupaten Bantul. *Rancang Bangun Teknik Sipil*, 7(1), 23–30.

[16] Fajarini, G. I., Purnamasari, I., & Wahyuningsih, S. (2018). Prediksi data curah hujan dengan menggunakan statistika non-parametrik. *Jurnal Eksponensial*, 9(2), 65–72.

[17] Rahmani, R. N., Sobriyah, & Wahyudi, A. H. (2020). Transformasi hujan harian ke hujan jam-jaman menggunakan metode Mononobe dan pengalihragaman hujan aliran (Studi Kasus di DAS Tirtomoyo). *Jurnal Matriks Teknik Sipil*, 8(1), 47–54.

[18] Sugawara, M. (1974). Hydrological models and their applications. *Hydrological Sciences Journal*, 19(3), 257–270.

[19] Chow, V. T., Maidment, D. R., & Mays, L. W. (1988). *Applied Hydrology*. New York: McGraw-Hill.

[20] Koutsoyiannis, D., & Manetas, A. (1996). Simple disaggregation by accurate adjustment. *Journal of Hydrology*, 182(1–4), 355–361.

[21] Wasono, A., Sari, Y. K., & Sangkawati, S. (2023). Analisis debit banjir berdasarkan data curah hujan pada DAS Sekampung menggunakan pemodelan HEC-HMS. *Jurnal Agregat*, 11(1), 45–54.

[22] Younis, J., & Siddiqui, M. A. (2015). Rainfall-runoff modeling using HEC-HMS for a semi-arid catchment in Pakistan. *Arabian Journal for Science and Engineering*, 40(5), 1525–1536.

[23] Ramadhan, N. A., Christuaji, A., & Santosa, B. (2024). Analisis kawasan banjir pada sungai menggunakan hydraulic model HEC-RAS 2D. *Prosiding Teknik Sipil Universitas Katolik Soegijapranata*, 2(1), 50–58.

[24] US Army Corps of Engineers. (2021). *HEC-RAS River Analysis System: Hydraulic Reference Manual Version 6.0*. Davis, CA: Hydrologic Engineering Center.

[25] Kumbier, K., Apel, H., & Thieken, A. H. (2018). Coupling 2D hydrodynamic modeling with tidal boundary conditions for coastal flood risk assessment. *Natural Hazards and Earth System Sciences*, 18(12), 3341–3357.

[26] Cahyono, C dan Adidarma, W. (2019), "Influence analysis of peak rate factor in the flood events' calibration process using HEC–HMS", *Modeling Earth Systems and Environment*, Vol. 5, No.4 Hal. 1705 – 1722.

[27] Supriyanto, B., & Nugroho, P. (2021). *Perbandingan Akurasi Prediksi Pasang Surut antara Metode Admiralty dan Least Square di Stasiun Surabaya*. Jurnal Geoid, 16(2), 67–74.

[28] Kurniawan, I., Damarnegara, S., & Margini, N. F. (2023). *Evaluation of Discharge Calculation in Open Pit Mining*. Jurnal Civil Engineering, 12(1), 13–19.